Rocksalt CeO epitaxial thin film as a heavy-fermion system transiting from *p*-type metal to partially compensated *n*-type metal by $4f$ delocalization

Nobuto Abe,[1] Daichi Oka,[1] Kenichi Kaminaga,[2,3] Daisuke Shiga,[4] Daichi Saito,[1] Taku Yamamoto,[1] Noriaki Kimura,[5] Hiroshi Kumigashira,[4,6] and Tomoteru Fukumura[1,2,7,8,*]

[1]*Department of Chemistry, Graduate School of Science, Tohoku University, Sendai 980–8578, Japan*
[2]*Advanced Institute for Materials Research (WPI-AIMR) and Core Research Cluster, Tohoku University, Sendai 980–8577, Japan*
[3]*Department of Applied Chemistry, School of Engineering, Tohoku University, Sendai 980–8579, Japan*
[4]*Institute of Multidisciplinary Research for Advanced Materials (IMRAM), Tohoku University, Sendai 980–8577, Japan*
[5]*Department of Physics, Graduate School of Science, Center for Low Temperature Science, Tohoku University, Sendai 980–8578, Japan*
[6]*Photon Factory, Institute of Materials Structure Science, High Energy Accelerator Research Organization (KEK), Tsukuba 305–0801, Japan*
[7]*Center for Science and Innovation in Spintronics, Organization for Advanced Studies, Tohoku University, Sendai 980–8577, Japan*
[8]*Center for Spintronics Research Network, Tohoku University, Sendai 980–8577, Japan*

(Received 27 April 2022; revised 19 August 2022; accepted 23 August 2022; published 6 September 2022)

Rocksalt CeO (001) epitaxial thin films were synthesized and their electronic properties were investigated. A simple $4f^1 5d^1$ electronic configuration with $4f$–$5d$ hybridization in CeO was confirmed by x-ray photoemission and absorption spectroscopy. While $5d$ conduction holes governed the metallic conduction at high temperatures, a partially compensated *n*-type conduction appeared below ~10 K with a rapid decrease in resistivity corresponding to a Fermi liquid state. The hole mobility was as high as 646 $cm^2 V^{-1} s^{-1}$ at 2 K in contrast to the two decades lower electron mobility, reflecting the large and small dispersion of $5d$ and $4f$ bands, respectively. At 0.8 K, a resistivity minimum was observed as a manifestation of the Kondo effect, indicating partial $4f$ localization. These results represented that the significant $4f$–$5d$ hybridization induced a Kondo coherent state in CeO with a short Ce-Ce interionic distance unlike the other antiferromagnetic Ce chalcogenides.

DOI: 10.1103/PhysRevB.106.125106

I. INTRODUCTION

Intermetallic Ce compounds have been widely studied as a heavy-fermion system containing significantly hybridized $4f$ and conduction electrons [1–3], generating fascinating electronic and magnetic phenomena such as extremely large effective charge-carrier mass in $Ce(Cu, Au)_6$ [4], multiple metamagnetic transitions in Ce monopnictides [5,6], heavy-fermion superconductivity in $CeCu_2Si_2$ [7], and energy gap formation via the Kondo effect in Ce_3Bi_4Pt [8]. Those rich electronic and magnetic phases generally reside in the Doniach phase diagram as a function of hybridization between the conduction and $4f$ electrons [9,10]. Strong hybridization makes the Kondo coupling dominate over the Ruderman–Kittel–Kasuya–Yosida interaction, stimulating itinerancy of $4f$ electrons at low temperatures.

So far, temperature-induced reconstruction of the Fermi surface in heavy-fermion systems has been intensively studied by various experimental techniques [11–13]. The Hall effect measurements have not been useful to evaluate quantitatively the amounts of charge carriers associated with the $4f$ delocalization because of the intricate Hall signals due to a large anomalous Hall effect and/or multiple band carriers [14,15]. Rocksalt-type Ce monochalcogenides Ce*Ch*s (*Ch* = O, S, Se, and Te) possess simple $4f^1 5d^1$ electronic configurations, and thus are suitable to investigate heavy-fermion phenomena via electrical measurements. For *Ch* = S, Se, and Te, the $5d$ conduction electrons contribute to the metallic conduction with local resistivity minima due to the Kondo effect, followed by the resistivity drop associated with an antiferromagnetic phase transition at lower temperatures [16]. The higher antiferromagnetic phase transition temperature for smaller anions in Ce*Ch* [CeS (8.4 K), CeSe (5.6 K), and CeTe (2.2 K) [17]] indicates that Ce*Ch* with smaller anions is closer to the quantum critical point. This chemical trend can be a consequence of a larger $4f$–$5d$ transfer integral and closer energy between the $4f$ and $5d$ bands for the smaller *Ch* anions [18], as seen in Ce monopnictides [19]. According to the Doniach phase diagram, Kondo coherent states dominate over the antiferromagnetism by applying external pressure in Ce*Ch* [16]. Therefore, the much smaller lattice constant of CeO (5.089 Å) than those of CeS (5.778 Å), CeSe (5.992 Å), and CeTe (6.36 Å) [17,20] would show a heavy-fermion state under the strongest $4f$–$5d$ hybridization. Indeed, a theoretical calculation predicted a semimetallic band structure, where the $5d$ and $4f$ bands formed hole and electron pockets around the Fermi level, respectively [21], suggesting the high hole mobility that is rare for oxides. However, CeO has not been synthesized for 40 years because of the difficulty in its synthesis due to unusual charge state of Ce^{2+} [20,22].

Recently, metastable rocksalt rare-earth monoxides have been synthesized for various rare-earth elements such as Y, La, Pr, Nd, Sm, Gd, Ho, Yb, and Lu by using pulsed laser

*tomoteru.fukumura.e4@tohoku.ac.jp

deposition [23–31]. In this study, we synthesized CeO epitaxial thin films and investigated their physical properties. CeO epitaxial thin films were paramagnetic metal and showed a Fermi liquid behavior below ∼10 K, where a transition from a *p*-type metal to a partially compensated *n*-type metal was induced by $4f$ delocalization. With further decreasing temperature down to 0.2 K, a Kondo effect was observed, indicating that a small portion of $4f$ electrons remained localized even at such low temperatures.

II. EXPERIMENT

CeO epitaxial thin films were synthesized on $YAlO_3$ (110) substrates at 250 °C by pulsed laser deposition. A Ce metal (99.9%) target was irradiated using a KrF excimer laser ($\lambda = 248$ nm) with a laser energy of 1.0 J/cm^2 and a repetition rate of 10 Hz in an ultrahigh vacuum chamber with a base pressure of $\sim 6 \times 10^{-9}$ Torr. Pure O_2 gas was supplied during the film synthesis with a partial pressure of 2.4×10^{-8} Torr, monitored by a quadrupole mass spectrometer. The typical film thickness measured by x-ray reflection was about 6 nm. In order to prevent film degradation, an amorphous AlO_x insulating layer (∼6 nm thick) was deposited *in situ* on the film at room temperature. The crystal structure was characterized by x-ray diffraction (XRD) with a four-axis diffractometer (D8 Discover, Bruker AXS). Hard x-ray photoelectron spectroscopy (HAXPES) was performed using an incident photon energy ($h\nu$) of 8 keV at the beamline BL47XU of the SPring-8. X-ray absorption spectroscopy (XAS) and soft x-ray photoemission spectroscopy (SXPES) were performed at the beamline BL-2A MUSASHI of the Photon Factory, KEK. All spectroscopic measurements were conducted at 300 K, and the Fermi level (E_F) was calibrated by the measurement of a gold film that was electrically connected to the sample. In the SXPES measurement, $h\nu$ was varied around the Ce $3d$–$4f$ threshold for resonant photoemission measurement, where $h\nu$s of on- and off-resonance were determined by measuring XAS at the Ce $M_{4,5}$ absorption edge. Electrical transport properties were evaluated for Hall-bar–shaped thin films by four-probe and Hall effect measurements from 2 K to 300 K and from 0.2 K to 1.3 K using a physical property measurement system (PPMS, Quantum Design) and a dilution refrigerator (Kelvinox TLM, Oxford Instruments), respectively. Magnetic properties were measured by a magnetic property measurement system (MPMS2, Quantum Design).

III. RESULTS AND DISCUSSION

Figure 1(a) shows a typical XRD $\theta - 2\theta$ pattern of the CeO thin film on $YAlO_3$ (110) substrate. The CeO 002 diffraction peak was observed without any impurity phase. The full width at half-maximum of the rocking curve around the CeO 002 peak was 0.08 °, representing the high crystallinity of the thin film [Fig. 1(a), inset]. A spot 224 diffraction peak in the two-dimensional reciprocal space map indicated coherent growth of the CeO epitaxial thin film [Fig. 1(b)]. The epitaxial relationship for the out-of-plane and in-plane directions was CeO (001) ∥ $YAlO_3$ (110) and CeO [110] ∥ $YAlO_3$ [001], respectively. The lattice constants of thin film were $a = 5.200$ Å and $c = 5.150$ Å, slightly larger than that of $a = 5.089$ Å for the bulk polycrystal [20]. The distances between the nearest-neighbor Ce ions in the CeO thin film were 3.68 Å and 3.64 Å along the in-plane and out-of-plane directions, respectively, exceeding the Hill limit of 3.41 Å for Ce [32]. Accordingly, the $4f$ orbitals would not be directly overlapped in the CeO thin films.

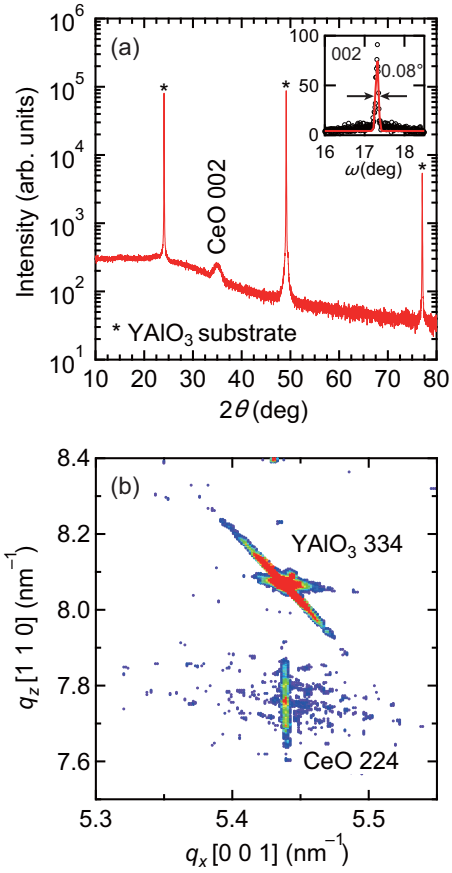

FIG. 1. (a) XRD θ–2θ pattern for CeO epitaxial thin film on $YAlO_3$ (110) substrate. The inset shows the rocking curve around the CeO 002 diffraction. (b) Reciprocal space map around 224 diffraction for the CeO epitaxial thin film.

In the HAXPES valence-band spectrum of the CeO thin film, the Ce $5d$ states were distributed within 3 eV below E_F, while the O $2p$ states were in the binding energies of 5 to 15 eV [Fig. 2(a)]. The existence of a clear Fermi edge indicated a metallic band structure of CeO with $5d$ conduction electrons or holes. In comparing the Ce $3d$ core-level spectrum of CeO taken by HAXPES with those of reference Ce metal and oxides with different oxidation states, the peak top of the $4f^1$ final-state peaks for the CeO thin film was located between those of Ce metal and Ce_2O_3 [Fig. 3(a)] [33,34], reflecting their intermediate charge state. The nature of trivalent Ce ions in metallic states for the CeO thin film were also supported by the XAS spectrum [Fig. 3(b)], where the obtained spectrum was similar to those reported for trivalent Ce intermetallic compounds [35].

To examine the $4f$–$5d$ hybridization in CeO, we next performed Ce $3d$–$4f$ resonant photoemission measurements. As shown in Fig. 2(b), the resonant spectra are reminiscent of the typical Ce intermetallic compounds [36], suggesting

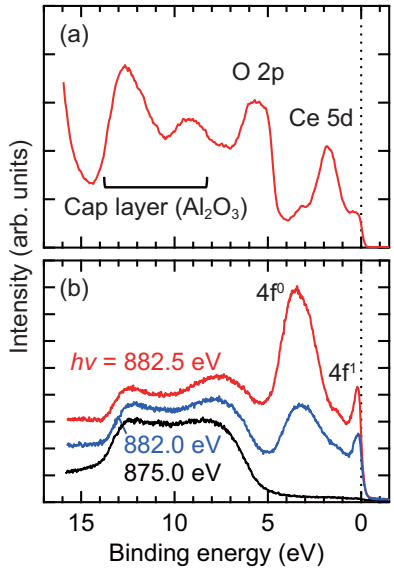

FIG. 2. Valence band photoemission spectra for an AlO_x-capped CeO epitaxial thin film taken by (a) HAXPES at $h\nu = 8$ keV and (b) SXPES at the energies around the Ce M-edge absorption edge. Because amorphous AlO_x is an insulator with a band gap of more than 6 eV, an AlO_x capping layer does not mask the electronic structures in the energy range from $E_F - 5$ eV to E_F derived from the Ce $5d$ and $4f$ states of the buried CeO film [25].

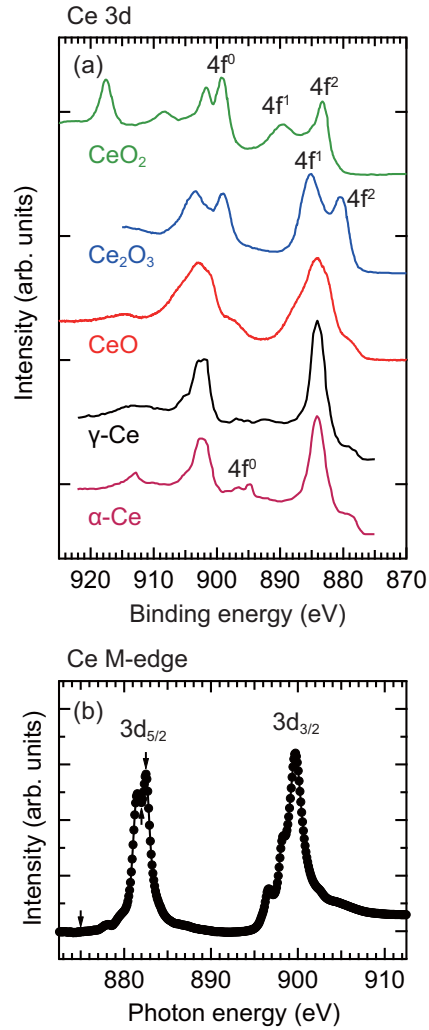

FIG. 3. (a) Ce $3d$ core-level spectrum obtained by hard x-ray photoemission and (b) x-ray absorption spectrum at the Ce M edge for CeO epitaxial thin film. Spectra for α-Ce, γ-Ce, Ce_2O_3, and CeO_2 are shown in (a) as references [33,34]. The arrows in (b) denote the energies used in the on- and off-resonant soft x-ray photoemission spectroscopy in Fig. 2(b).

the substantial hybridization between the $4f$ level and the $5d$ conduction band. Two clear, resonant enhanced peaks were observed at E_F and 3.5 eV below E_F on-resonance ($h\nu = 882.0$ eV and 882.5 eV) [Fig. 2(b)] in comparison with off-resonance ($h\nu = 875$ eV). The sharp peak just at E_F corresponds to the so-called Kondo resonance peaks of the excitation to the $4f^1$ ($4f^1 \rightarrow 4f^1\underline{c}$) final state ($\underline{c}$: a hole in the $5d$ conduction band), while the relatively broad peak centered around 3.5 eV is the excitation to the $4f^0$ ($4f^1 \rightarrow 4f^0$) final state, respectively [37]. The former indicated itinerancy of the $4f$ electrons through $4f$–$5d$ hybridization, although the areal fraction of the $4f^1$ peak in total intensity of $4f^0 + 4f^1$ peaks is small. The latter is close to the bare state of the $4f$ level, energetically overlapping with the $5d$ states. From these results, the Ce ion in CeO was almost trivalent, possessing an approximate $4f^1 5d^1$ configuration with weak but finite $4f$–$5d$ hybridization, being consistent qualitatively with the previous band calculation [21].

Figure 4(a) shows temperature (T) dependence of electrical resistivity ρ_{xx} for the CeO thin film from 2 K to 300 K. The ρ_{xx}–T curve during upward and downward T sweeps was reversible without any hysteresis, unlike Ce metal [38], confirming no Ce metal impurity in the film. The metallic behavior ($d\rho_{xx}/dT > 0$) was consistent with the metallic band structure observed in HAXPES [Fig. 2(a)]. Below a characteristic temperature T^* of ~10 K, ρ_{xx} decreased rapidly proportional to T^2 with a coefficient A of 0.219 $\mu\Omega$ cm K^{-2} [Fig. 4(a), inset], exhibiting a Fermi liquid behavior. Similar to the other heavy-fermion compounds [39–41], the resistivity drop was concomitant with the sign change in magnetoresistance at 9 T from negative to positive [Fig. 4(a)]. This unconventional T dependence of ρ_{xx} is in contrast to the featureless ρ_{xx}–T curve in the normal state of superconducting LaO without the $4f$ electron [24], indicating significant influences of the $4f^1$ electron on the electrical conduction in CeO. According to the Fermi liquid theory, $A^{-1/2}$ is proportional to the Kondo temperature T_K [42], while a relationship of $T_K \propto A^{-1/3}$ was seen in Ce-based heavy-fermion compounds as well as CeO [43–50], as summarized in Supplemental Material Fig. S1 [51], assuming $T_K = 75$ K estimated for CeO from a bulk modulus measurement [22]. Those results indicated that the significant $4f$–$5d$ hybridization due to the short Ce interionic distance induced not antiferromagnetism like the other CeChs, but a Kondo coherent state in CeO, as expected from the Doniach phase diagram.

With further decreasing temperature, ρ_{xx} showed a minimum around 0.8 K followed by a slight increase proportional to ln$T$ as a manifestation of the Kondo effect [Fig. 4(b)], whose origin was different from that in the previously mentioned Kondo coherent state. The possibility of weak

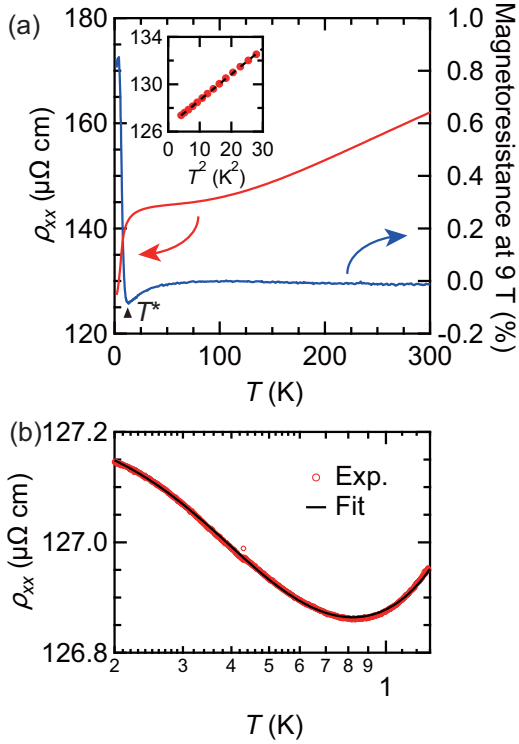

FIG. 4. (a) T dependence of ρ_{xx} and magnetoresistance at 9 T from 2 K to 300 K for CeO epitaxial thin film. The triangle denotes T^*. The inset shows ρ_{xx} as a function of T^2 from 2 K to 9 K. The dotted line is a linear fit. (b) T dependence of ρ_{xx} from 0.2 K to 1.3 K for CeO epitaxial thin film. The fitting result with Eq. (1) is also shown (black curve).

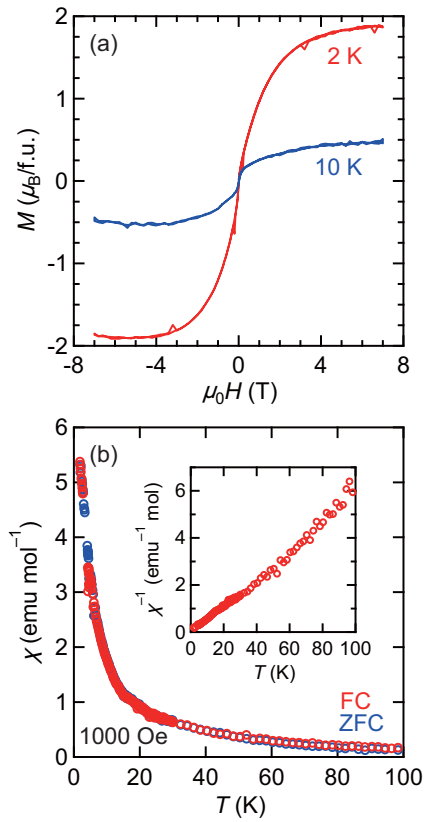

FIG. 5. (a) Magnetization curves at 2 K and 10 K and (b) temperature dependence of magnetic susceptibility under field-cooled and zero-field–cooled conditions for CeO epitaxial thin film. The inset in (b) shows inversed magnetic susceptibility as a function of temperature. The magnetic field was applied along the in-plane direction.

localization was ruled out by the positive parabolic magnetoresistance even at around 25 mK, as seen in Supplemental Material Fig. S2 [51]. Here, the ρ_{xx} can be expressed as $\rho_{xx} = \rho_r + AT^n + \rho_K$, where ρ_r is the residual resistivity, the second term is the metallic component toward the Fermi liquid state, and ρ_K is the Kondo resistivity. ρ_K is described by the following Hamann's equation [52],

$$\rho_K = \frac{\rho_0}{2}\left\{1 - \frac{\ln(T/T_{K'})}{\left[\ln^2(T/T_{K'}) + S(S+1)\pi^2\right]^{1/2}}\right\}, \qquad (1)$$

where ρ_0 is the unitarity limit, T_K' is the Kondo temperature for the low-temperature Kondo scattering, and S is the spin of the magnetic impurity. The ρ_{xx}–T curve below 2.0 K was well fitted to Eq. (1) [Fig. 4(b)], yielding a T_K' of 0.423 K and an S of 0.087. Similar small S parameters were reported for various Ce-based Kondo compounds probably due to the crystal field effects and orbital degeneracy [53–55]. This result suggested that the Kondo effect originated from partially localized $4f$ electrons of Ce even in the Kondo coherent state, although we cannot fully rule out the possible contribution of the small amount of unintentional magnetic impurities.

Magnetism of the CeO thin film was investigated by magnetization measurements. The magnetization curves at 2 K and 10 K did not show any hysteresis [Fig. 5(a)]. The temperature dependence of field-cooled and zero-field–cooled magnetic susceptibility almost overlapped [Fig. 5(b)], where the inversed magnetic susceptibility was proportional to temperature. Hence, the CeO thin films was paramagnetic down to 2 K. The large saturation magnetization at 2 K could be attributed to Pauli paramagnetism due to the $5d$ electrons, similar to the other paramagnetic Ce-based heavy-fermion compounds [44,56]. The lack of magnetic ordering supported that the CeO thin film resided in the delocalization regime of the Doniach phase diagram.

Hall effect and magnetoresistance were measured at different temperatures to evaluate the carrier density and mobility [Fig. 6(a)]. At 10 K and higher, the Hall resistivity ρ_{yx} showed positively linear magnetic field dependence, indicating a simple p-type metallic conduction. The p-type character was also seen in the other Ce monochalcogenides [17]. Below 10 K, on the other hand, nonlinear magnetic field dependence of ρ_{yx} was observed, accompanied by relatively large, positive magnetoresistance [Fig. 6(b)]. This nonlinear magnetic field dependence was probably caused by the presence of p-type and n-type carriers, considering the lack of magnetic ordering down to 2 K. Indeed, the magnetic field dependences of ρ_{yx} and ρ_{xx} at 2 K and 5 K were well fitted by the two-carrier Drude model [Figs. 6(a) and 6(b), insets], validating the presence of both conduction electrons and holes.

Figure 7 shows the electron and hole carrier density and mobility as a function of temperature. At 10 K and higher,

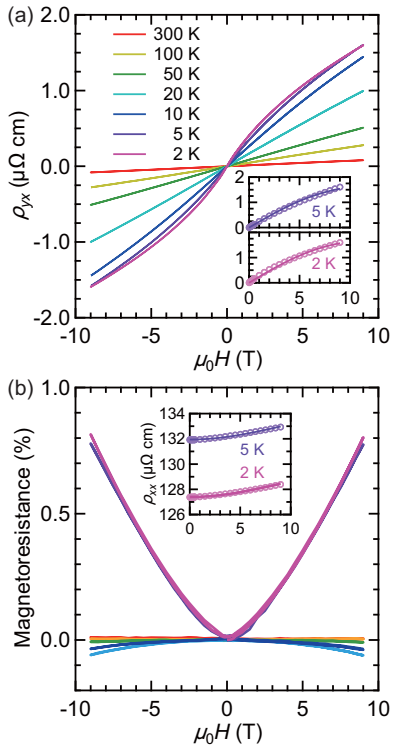

FIG. 6. Magnetic field dependence of (a) Hall resistivity and (b) magnetoresistance for CeO epitaxial thin film. Insets of (a) and (b) show the fitting results (solid lines) by the two-carrier Drude model.

only high-density hole carriers on the order of $10^{22}\,\mathrm{cm}^{-3}$ were present. Below 10 K, high-density conduction electrons emerged whereas the conduction holes abruptly decreased with a dramatic increase in mobility of up to $646\,\mathrm{cm}^2\,\mathrm{V}^{-1}\,\mathrm{s}^{-1}$ at 2 K. The two-decades higher hole mobility than the electron mobility reflected the much larger dispersion of the $5d$ band than that of the $4f$ band. This electronic transition occurred at $T^* = \sim 10\,\mathrm{K}$, where ρ_{xx} showed the steep drop [Fig. 4(a)].

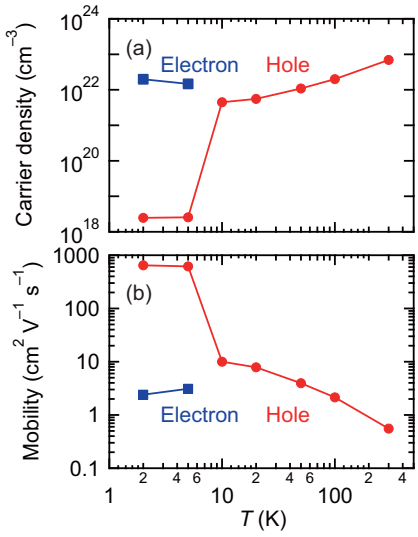

FIG. 7. T dependence of (a) electron (square) and hole (circle) carrier density and (b) mobility for CeO epitaxial thin film.

The electron density of $1.98 \times 10^{22}\,\mathrm{cm}^{-3}$ at 2 K was close to the nominal $4f$ electron density of $2.87 \times 10^{22}\,\mathrm{cm}^{-3}$ in the $4f^1$ configuration, indicating significant delocalization of $4f$ electrons.

Here, we discuss the possible origin of the phase transition from a p-type metal to a partially compensated n-type metal in the CeO thin film. At high temperatures above T^*, the $4f$ electrons were fully localized because of the weak $4f$–$5d$ hybridization as observed by SXPES. Thus, the $5d$ conduction holes dominated the electrical conduction, which is qualitatively consistent with the calculated band structure with a large hole pocket [21]. With decreasing temperature down to T^*, the enhanced hybridization would open a gap state in the $5d$ band [57], leading to the significant decrease in the $5d$ conduction holes. At the same time, the majority of the $4f$ electrons delocalized, as described earlier. The slightly lower carrier density than the nominal $4f$ electron density also indicated that a small fraction of $4f$ electrons remained localized even below T^*, which could induce the Kondo effect at such low temperatures [Fig. 4(b)].

IV. CONCLUSION

CeO (001) epitaxial thin films on $YAlO_3$ (110) substrates were synthesized by pulsed laser deposition. X-ray photoemission and absorption spectroscopy indicated a $4f^1 5d^1$ electronic configuration with relatively weak $4f$–$5d$ hybridization. The CeO thin film showed p-type metallic conduction at high temperatures and phase transition to a partially compensated n-type metal with a Fermi liquid behavior at $T^* = \sim 10\,\mathrm{K}$. The electrical conduction below T^* was well explained by the two-carrier Drude model reflecting the simple electronic configuration of CeO. The high (low) carrier density and low (high) mobility of conduction electrons (holes) suggested gap formation in the $5d$ band due to the $4f$–$5d$ hybridization at T^*. At significantly lower temperatures than T^*, the Kondo effect was probably caused by the small fraction of $4f$ electrons remaining localized. Further investigations such as low-temperature photoemission spectroscopy would elucidate the band structure associated with the transition from a p-type metal to a partially compensated n-type metal in CeO.

ACKNOWLEDGMENTS

This work was financially supported by Grants-in-Aid for Scientific Research (Grants No. 18H03872, No. 18K18935, No. 19K15440, No. 19F19347, No. 20H02704, and No. 21H05008) from the Japan Society for the Promotion of Science (JSPS), and CREST (Grant No. JPMJCR18T1) from the Japan Science and Technology Agency (JST). The hard x-ray photoemission measurements at SPring-8 were conducted under approval of the Japan Synchrotron Radiation Research Institute (Approval No. 2019B1248). The work performed at KEK-PF was approved by the Program Advisory Committee (Proposals No. 2018S2-004 and No. 2021S2-002) at the Institute of Materials Structure Science, KEK.

[1] G. R. Stewart, Rev. Mod. Phys. **56**, 755 (1984).
[2] P. Coleman, C. Pépin, Q. Si, and R. Ramazashvili, J. Phys. Condens. Matter **13**, R723 (2001).
[3] P. Gegenwart, Q. Si, and F. Steglich, Nat. Phys. **4**, 186 (2008).
[4] A. Schröder, G. Aeppli, R. Coldea, M. Adams, O. Stockert, H. V. Löhneysen, E. Bucher, R. Ramazashvili, and P. Coleman, Nature (London) **407**, 351 (2000).
[5] T. Inoue, T. Kuroda, K. Sugiyama, Y. Haga, T. Suzuki, and M. Date, J. Phys. Soc. Jpn. **64**, 572 (1995).
[6] J. Rossat-Mignod, P. Burlet, S. Quezel, J. M. Effantin, D. Delacôte, H. Bartholin, O. Vogt, and D. Ravot, J. Magn. Magn. Mater. **31–34**, 398 (1983).
[7] F. Steglich, J. Aarts, C. D. Bredl, W. Lieke, D. Meschede, W. Franz, and H. Schäfer, Phys. Rev. Lett. **43**, 1892 (1979).
[8] M. F. Hundley, P. C. Canfield, J. D. Thompson, Z. Fisk, and J. M. Lawrence, Phys. Rev. B **42**, 6842 (1990).
[9] S. Doniach, Physica B+C **91**, 231 (1977).
[10] S. Hoshino and Y. Kuramoto, Phys. Rev. Lett. **111**, 026401 (2013).
[11] P. T. Coleridge, J. Phys. F Met. Phys. **17**, L79 (1987).
[12] S. K. Goh, J. Paglione, M. Sutherland, E. C. T. O'Farrell, C. Bergemann, T. A. Sayles, and M. B. Maple, Phys. Rev. Lett. **101**, 056402 (2008).
[13] S. Jang, J. D. Denlinger, J. W. Allen, V. S. Zapf, M. B. Maple, J. N. Kim, B. G. Jang, and J. H. Shim, Proc. Natl. Acad. Sci. **117**, 23467 (2017).
[14] S. Nair, S. Wirth, S. Friedemann, F. Steglich, Q. Si, and A. J. Schofield, Adv. Phys. **61**, 583 (2012).
[15] K. Winzer, Z. Phys. B Condens. Matter **64**, 159 (1986).
[16] Y. Hayashi, S. Takai, T. Matsumura, H. Tanida, M. Sera, K. Matsubayashi, Y. Uwatoko, and A. Ochiai, J. Phys. Soc. Jpn. **85**, 034704 (2016).
[17] F. Hulliger, B. Natterer, and H. R. Ott, J. Magn. Magn. Mater. **8**, 87 (1978).
[18] M. Nakayama, H. Aoki, A. Ochiai, T. Ito, H. Kumigashira, T. Takahashi, and H. Harima, Phys. Rev. B **69**, 155116 (2004).
[19] A. Fujimori and J. H. Weaver, Phys. Rev. B **31**, 6345 (1985).
[20] J. M. Leger, N. Yacoubi, and J. Loriers, J. Solid State Chem. **36**, 261 (1981).
[21] S. K. De and S. Chatterjee, J. Phys. Condens. Matter **1**, 1169 (1989).
[22] J. M. Léger, Physica B **190**, 84 (1993).
[23] K. Kaminaga, R. Sei, K. Hayashi, N. Happo, H. Tajiri, D. Oka, T. Fukumura, and T. Hasegawa, Appl. Phys. Lett. **108**, 122102 (2016).
[24] K. Kaminaga, D. Oka, T. Hasegawa, and T. Fukumura, J. Am. Chem. Soc. **140**, 6754 (2018).
[25] H. Shimizu, D. Oka, K. Kaminaga, D. Saito, T. Yamamoto, N. Abe, N. Kimura, D. Shiga, H. Kumigashira, and T. Fukumura, Phys. Rev. B **105**, 014442 (2022).
[26] D. Saito, K. Kaminaga, D. Oka, and T. Fukumura, Phys. Rev. Mater. **3**, 064407 (2019).
[27] Y. Uchida, K. Kaminaga, T. Fukumura, and T. Hasegawa, Phys. Rev. B **95**, 125111 (2017).
[28] T. Yamamoto, K. Kaminaga, D. Saito, D. Oka, and T. Fukumura, Appl. Phys. Lett. **117**, 052402 (2020).
[29] T. Amrillah, D. Oka, H. Shimizu, S. Sasaki, D. Saito, K. Kaminaga, and T. Fukumura, Appl. Phys. Lett. **120**, 082403 (2022).
[30] T. Yamamoto, K. Kaminaga, D. Saito, D. Oka, and T. Fukumura, Appl. Phys. Lett. **114**, 162104 (2019).
[31] K. Kaminaga, D. Oka, T. Hasegawa, and T. Fukumura, ACS Omega **3**, 12501 (2018).
[32] J. Tang and K. A. Gschneidner, J. Less Common Met. **149**, 341 (1989).
[33] R. Eloirdi, P. Cakir, F. Huber, A. Seibert, R. Konings, and T. Gouder, Appl. Surf. Sci. **457**, 566 (2018).
[34] E. Wuilloud, H. R. Moser, W.-D. Schneider, and Y. Baer, Phys. Rev. B **28**, 7354 (1983).
[35] L. Howald, E. Stilp, P. D. de Réotier, A. Yaouanc, S. Raymond, C. Piamonteze, G. Lapertot, C. Baines, and H. Keller, Sci. Rep. **5**, 12528 (2015).
[36] E. Weschke, C. Laubschat, T. Simmons, M. Domke, O. Strebel, and G. Kaindl, Phys. Rev. B **44**, 8304 (1991).
[37] O. Gunnarsson and K. Schönhammer, Phys. Rev. B **28**, 4315 (1983).
[38] P. Burgardt, K. A. Gschneidner, D. C. Koskenmaki, D. K. Finnemore, J. O. Moorman, S. Legvold, C. Stassis, and T. A. Vyrostek, Phys. Rev. B **14**, 2995 (1976).
[39] G. Remenyi, A. Briggs, J. Flouquet, O. Laborde, and F. Lapierre, J. Magn. Magn. Mater. **31–34**, 407 (1983).
[40] A. Sumiyama, Y. Oda, H. Nagano, Y. Ōnuki, K. Shibutani, and T. Komatsubara, J. Phys. Soc. Jpn. **55**, 1294 (1986).
[41] N. Kawakami and A. Okiji, J. Phys. Soc. Jpn. **55**, 2114 (1986).
[42] S. Raymond and D. Jaccard, J. Low Temp. Phys. **120**, 107 (2000).
[43] H. R. Ott, H. Rudigier, Z. Fisk, J. O. Willis, and G. R. Stewart, Solid State Commun. **53**, 235 (1985).
[44] H. G. Schlager, A. Schröder, M. Welsch, and H. v. Löhneysen, J. Low Temp. Phys. **90**, 181 (1993).
[45] P. Haen, J. Flouquet, F. Lapierre, P. Lejay, and G. Remenyi, J. Low Temp. Phys. **67**, 391 (1987).
[46] M. J. Besnus, J. P. Kappler, P. Lehmann, and A. Meyer, Solid State Commun. **55**, 779 (1985).
[47] D. Gignoux, F. Givord, R. Lemaire, and F. Tasset, J. Less Common Met. **94**, 165 (1983).
[48] Y. Ōnuki, T. Yamazaki, T. Omi, I. Ukon, A. Kobori, and T. Komatsubara, J. Phys. Soc. Japan **58**, 2126 (1989).
[49] J. D. Thompson, J. M. Lawrence, and Z. Fisk, J. Low Temp. Phys. **95**, 59 (1994).
[50] I. Umehara, Y. Kurosawa, N. Nagai, M. Kikuchi, K. Satoh, and Y. Ōnuki, J. Phys. Soc. Japan **59**, 2848 (1990).
[51] See Supplemental Material at http://link.aps.org/supplemental/10.1103/PhysRevB.106.125106 for A vs. T_K for various Ce-based paramagnetic Kondo compounds, and magnetoresistance below 2 K for CeO epitaxial thin film.
[52] D. R. Hamann, Phys. Rev. **158**, 570 (1967).
[53] M. Dietrich, W. Gey, and E. Umlauf, Solid State Commun. **11**, 655 (1972).
[54] K. Winzer, Solid State Commun. **16**, 521 (1975).
[55] T. Komatsubara, N. Sato, S. Kunii, I. Oguro, Y. Furukawa, Y. Onuki, and T. Kasuya, J. Magn. Magn. Mater. **31–34**, 368 (1983).
[56] Y. Ōnuki, Y. Shimizu, and T. Komatsubara, J. Phys. Soc. Jpn. **54**, 304 (1985).
[57] S. Pal, C. Wetli, F. Zamani, O. Stockert, H. v. Löhneysen, M. Fiebig, and J. Kroha, Phys. Rev. Lett. **122**, 096401 (2019).